Catalysis Today 159 (2011) 108–119

Contents lists available at ScienceDirect

Catalysis Today

journal homepage: www.elsevier.com/locate/cattod

Rapid optical screening technology for direct methanol fuel cell (DMFC) anode and related electrocatalysts

F.G. Welsch, K. Stöwe, W.F. Maier*

Lehrstuhl für Technische Chemie, Universität des Saarlandes, Gebäude C4 2, 66123 Saarbrücken, Germany

ARTICLE INFO

Article history:
Available online 13 April 2010

Keywords:
Optical screening
High-throughput
DMFC catalysts
Acid stability
Electrocatalyst

ABSTRACT

We describe here the development of an optical high-throughput screening method for direct methanol fuel cell catalysts based on the fluorescence of protonated quinine generated during electro-oxidation of methanol. The design of the working electrode allows the parallel quantification of the fluorescence development for up to 60 materials. For the preparation of the working electrode a coating routine has been developed, which allows the use of sol–gel derived materials. Due to the required stability of the electrode catalysts towards the acidic polymer membrane, a fast optical pre-screening method for acid stable materials has been developed. The electrochemical high-throughput system has been validated with Pt-Ru catalysts. Automation of data acquisition and data processing led to a fast and reliable high-throughput screening setup.

1. Introduction

The direct methanol fuel cell (DMFC) is an alternative for a decentralized power supply. The high power density of methanol in combination with a low operating temperature and the possibility to incorporate compact membrane electrode assemblies (MEAs) in the DMFC makes this type of fuel cell applicable for a variety of technical areas, especially mobile devices such as mobile phones, PDAs, laptops or even for electric vehicles. Compared to hydrogen-based fuel cells no reforming unit or high pressure storage tank is needed. In addition, the compatibility of methanol with the existing petrol distributions system may become a key aspect for potential future applications of the DMFC.

A DMFC MEA consists of a cathode and an anode divided by a proton conducting polymer electrolyte membrane (PEM). Nafion, a copolymer of a tetrafluoroethylene and perfluorinated vinyl-ether comonomer [1], is commonly used as PEM. Due to its sulfonic-acid groups, Nafion determines the milieu of the catalyst/polymer membrane interface (pH ~ 1) [2]. Therefore, the corrosion resistance of the electrodes is absolutely required. Flow field plates, positioned next to the electrodes, provide the oxygen and the aqueous solution of methanol. Oxygen is reduced to water (Eq. (1)) at the cathode while methanol is oxidized to carbon dioxide at the anode by its electrode catalyst (Eq. (2)).

$$1.5O_2 + 6H^+ + 6e^- \leftrightarrows 3H_2O \quad (1)$$

$$CH_3OH + H_2O \leftrightarrows CO_2 + 6H^+ + 6e^- \quad (2)$$

$$1.5O_2 + CH_3OH \leftrightarrows CO_2 + 2H_2O$$

Among pure metals, platinum shows the best activity for the electro-oxidation of methanol at temperatures below 80 °C [3,4]. In the course of methanol electro-oxidation, platinum is poisoned by carbon monoxide (CO), an intermediate product adsorbed on the catalyst surface (Eq. (3)). Hydroxyl groups (OH), originated by water activation, oxidatively remove the adsorbed CO. Water activation on the platinum surface is responsible for a high over potential for the electro-oxidation of methanol on pure platinum [5].

$$Pt + CH_3OH \rightarrow Pt\text{-}CO_{ads} + 4H^+ + 4e^- \quad (3)$$

$$Ru + H_2O \rightarrow Ru\text{-}OH_{ads} + H^+ + e^- \quad (4)$$

$$Ru\text{-}OH_{ads} + Pt\text{-}CO_{ads} \rightarrow CO_2 + Pt + Ru + H^+ + e^- \quad (5)$$

In order to decrease the over potential due to the water activation platinum was alloyed with oxophilic metals. Among them, binary platinum-ruthenium (PtRu) alloys show the best activity for the electro-oxidation of methanol [5], but still methanol-oxidation kinetics is sluggish because ruthenium does not adequately activate water (Eq. (4)) [6]. Eqs. (3)–(5) illustrate the bi-functional mechanism of the electro-oxidation of methanol.

The high noble metal contents of the DMFC cathode and the PtRu-anode in combination with the slow reaction kinetics of electrode reactions [7] exhibit the economic weakness of the DMFC as a ubiquitous decentralized mobile power source. Present research activity concentrates on the optimization of the PtRu catalyst system through composition, surface area, particle size, morphology,

* Corresponding author. Tel.: +49 6 81 302 2422.
E-mail address: w.f.maier@mx.uni-saarland.de (W.F. Maier).

0920-5861/$ – see front matter © 2010 Elsevier B.V. All rights reserved.
doi:10.1016/j.cattod.2010.03.006

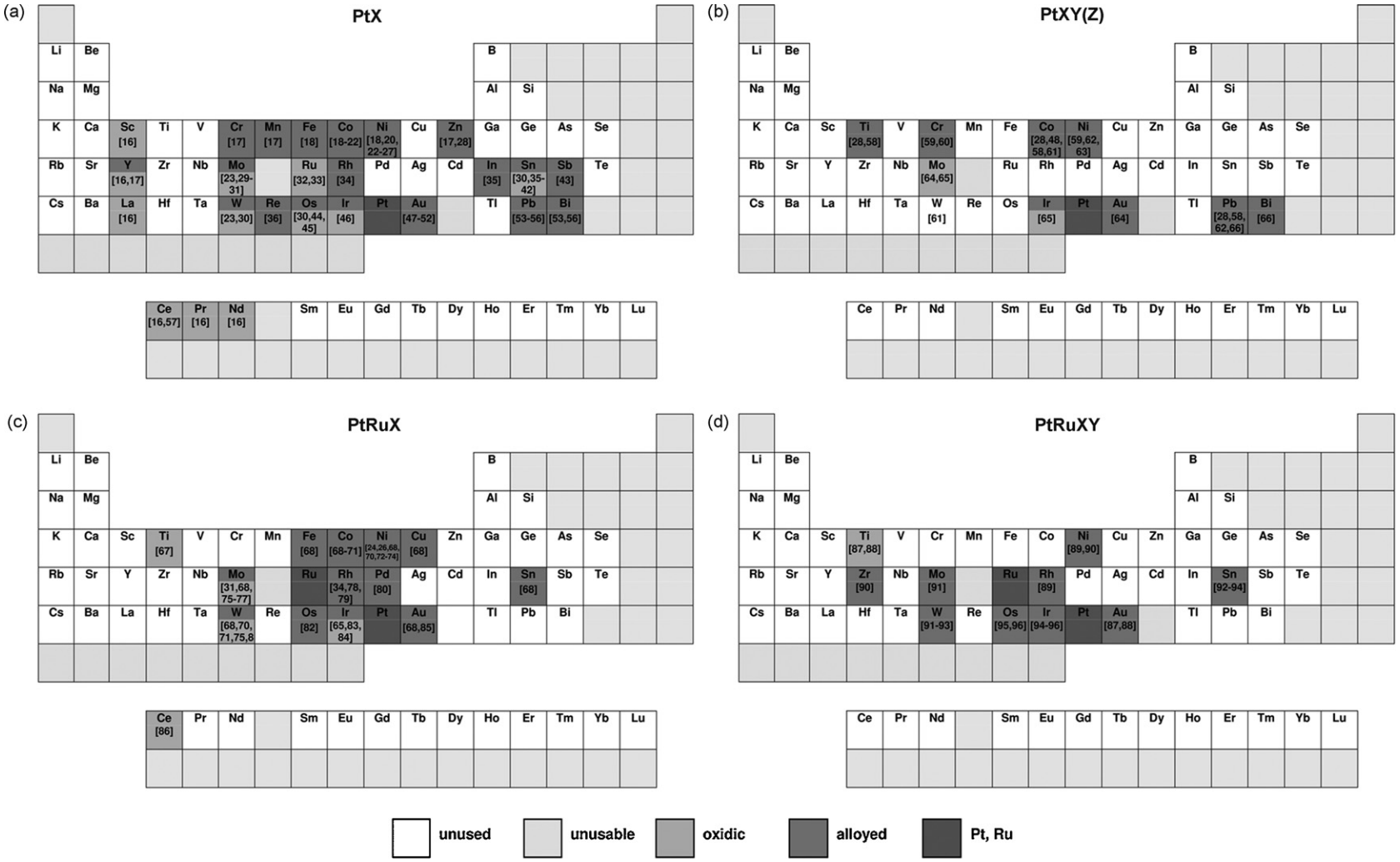

Fig. 1. Overview over the existing elemental compositions of DMFC anode catalysts of (a) PtX, (b) PtXY(Z), (c) PtRuX and (d) PtRuXY. Elements are labelled whether reported as oxidic phase or alloyed with the Pt, Ru; unused and unusable. Associated literature is referenced [16–27,29,30–52,54–57,60–65,67,68,70,72–78,80,81–86,88,89,92–94,96].

dispersion on different carriers, reduction of the noble metal content and increase in activity [8–15] as well as on the search for new or alternative elemental compositions of anode catalysts. Based on the established system PtRu, without regarding the oxidic or alloyed state of the added element, four main strategies can be identified from the literature:

- Ruthenium is replaced by another element (PtX, Fig. 1a).
- Ruthenium is substituted by up to three elements to form ternary or quaternary systems (PtXY(Z), Fig. 1b).
- One element is added to the PtRu system, leading to ternary systems (PtRuX, Fig. 1c).
- Two elements are added to the PtRu system, resulting in quaternary systems (PtRuXY, Fig. 1d).

Fig. 1 reviews the existing elemental compositions of DMFC anode catalysts of PtX, PtXY(Z), PtRuX and PtRuXY. The associated elements are labelled whether reported as oxidic phase or alloyed with the Pt, Ru; unused and unusable elements with associated references are given [16–27,29,30–52,54–57,60–65,67,68,70,72–78,80,81–86,88,89,92–94,96]. Some of the elemental combinations shown in Fig. 1 were widely researched by the use of different high-throughput (HT) methods to accelerate the process of catalyst optimization. These HT methods can be divided into two groups based on the screen used for the detection of active materials. The first group is based on the measurement of current or potential variations during the electro-oxidation of methanol [59,69,71,90,97–100]. One limiting factor for the array size and therefore the size of the materials library that can be measured at once, is the complex and costly hardware needed [101]. In contrast to this group, high-throughput setups based on the detection of optical effects induced by consecutive reactions of the protons produced during the methanol conversion are an attractive alternative with respect to hardware complexity. Reddington et al. published the fundamental work in 1998 [95]. Based on the transformation of quinine (at neutral pH) and the Ni^{2+} complex of 3-pyridin-2yl-[4,5,6]triazolo[1,5-a]pyridine (at low pH) in a protonated, fluorescent-active form during the drop of the pH resulting from methanol conversion, the optimum compositions of quaternary alloys have been successfully identified. The authors have essentially deposited composition gradients as films on top of conducting carbon papers as working electrode and monitored fluorescence during methanol oxidation. In a comparison of high-throughput electrochemical methods for DMFC anode catalyst development the optical screening method was mentioned to be effective in ranking for high and low activity and for surveys with large numbers of materials [102]. Mapping of active regions on a working electrode array and optimization of catalyst compositions have been reported by such fluorescence experiments [53,58,79,87,91]. The charm of such a method is its simplicity. The major drawback of such simple fluorescence experiments is the lack of quantification; it provides only yes/no answers. Since fluorescence of quinine solely depends on the number of protons released by methanol oxidation, quantification of the fluorescence signal during a potential sweep should be possible. We set out to do so and published first results of our work in September 2008 in the 5th International Conference on Combinatorial and High-Throughput Materials Science in Seeon, Bavaria. In 2007 Jin et al. [66], followed by Gregoire et al. [28], published the first semi-quantitative observation of the fluorescence development during a potential sweep.

In this work, we first combine the versatility of the sol–gel process with respect to automation and elemental compositions of the achieved materials [103] with an optical screening method for DMFC catalyst based on the work by Reddington et al. All catalyst materials studied here are free of any noble metal, while all materials found in the literature (references in Fig. 1) are doped Pt/Ru catalysts, either as alloys or oxides. Apparently there are no reports of mixed oxides in the literature in connection with fuel cell electrodes. We developed a setup and a coating procedure tailored to the needs of the obtained mixed oxides and the reduced materials thereof. For a fast detection of materials corroding in the acidic media, we developed a fast and reliable pre-screening method to reduce the number of electrochemical measurements. A special working electrode design allowed the quantification of the fluorescence intensity by the protonated quinine species during the methanol conversion.

2. Materials and methods

2.1. Commonly used materials

For all fluorescence based measurements the electrolyte solution was composed of 100 μM quinine (Fluka), 1 M methanol (Sigma–Aldrich) and 0.1 M sodium sulfate (Sigma–Aldrich). All experiments were performed in deionised water (Elga Purelab UVF, Elga Labwater). The fluorescence emission was excited by a UV lamp at 365 nm (VL-115 L, 15 W, UV Consulting Peschl). A potentiostat was used to control the potential of the working electrode arrays (PP 220, Zahner Elektronik). If not further specified, a platinum net was used as counter electrode and a $Hg/HgSO_4$ electrode (Ref 621, Radiometer Analytical) as reference electrode. All potentials were reported versus (vs.) the standard hydrogen electrode (SHE). Microscopic images were obtained using a Nikon Optiphot-2 microscope, equipped with a CCD camera (UEye LE, Ids Imaging).

2.2. Notation and synthesis of compounds

A simple notation was used to name the examined materials, for example, a binary mixture or binary mixed oxide is indicated by the contraction A_xB_{100-x} generally. A and B denote a particular element, the lower case x describes the molar fraction of the respective element in mol % not accounting for the oxidation states of the elements in the compound and thus not for any oxide content. Consequently, the mixture may be either metallic or oxidic or a mixture of both. Materials processed before reduction in H_2 are marked with the abbreviation O_x.

1300 transition metal containing materials were synthesized by a modified sol–gel process as described previously [104–106]. Synthesis was planned and controlled by the software Plattenbau [107] and carried out with the help of a pipetting robot (Zinsser Lissy). Mixed oxides were obtained after calcination and reduced materials after a reduction step in pure hydrogen as described below.

For the synthesis of $Pt_{50}Ru_{50}$, 1.0 ml of a 0.1 M solution of ruthenium-(III)-acetylacetonate (Sigma–Aldrich) and 0.4 ml of a 0.25 M solution of tetraamineplatin-(II)-acetate (Umicore) in a mixture of isopropanol and propionic acid (1:1, v/v) were mixed in 2 ml GC vials. After mixing, the sample was placed in an orbital shaker (Titramax 100, Heidolph) for 1 h. The sample was dried for 2 days at room temperature and for additional 8 days at 40 °C. The sample was calcined under static air at 250 and 400 °C for 5 h at both temperatures (heating rate 30 °C/h). After calcination, the sample was reduced under pure hydrogen in an oven with gas supply (VMK-80-Vac, Linn Hightherm, 50 ml/min) at 450 °C for 1 h (heating rate 13 °C/min).

2.3. Optical pre-screening for acid stability

Acid stability testing was carried out using 96-well plates (Greiner Bio). The wells of the plates were filled with approximately 5 mg of the compounds of interest in powder form. Subsequently 250 μl of a 1 M H_2SO_4 solution (Analytical Standard, Riedel de Haen) was added to each well. The well plates were positioned on an

orbital shaker for 1 h. Additionally, five wells of the plate were filled with the pure acid solution for reference. Images were acquired using a scanner (ScanMaker X 12 USL, Mustek) and commercially available acquisition software. Comparable light conditions were guaranteed by the use of a tailor-made well-plate lid, which allowed the reproducible positioning of the plate on the scanner. Images were acquired directly after the addition of the sulfuric acid solution and after 1, 3, 24, 48 and 72 h of acid contact time.

2.4. Cutting and Teflon coating of the graphite plates

The structured graphite plate was designed with commercial available CAD software. The structure was cut by a CNC machine using 150 mm × 150 mm × 15 mm and 75 mm × 75 mm × 15 mm graphite plates (Graphite Cova), respectively. Teflon coating was performed using a reverse dip coating procedure. A 60 wt% Teflon suspension was diluted 1:1 with deionised water, stirred for 10 min and filled into the cut wells and channels so that the walls between wells were covered up to the upper edge to gain a uniform sealing of the graphite plate electrolyte interface. Due to the porosity of the graphite plates some suspension liquid leaked through the plate after a certain period of time. Thus, after a contact time of 30 s the Teflon suspension was removed using a water-driven pump. The residual Teflon suspension was blown off by a N_2 flow. Drying was carried out under static air at 107 °C for 2 h at a heating rate of 1 °C/h. For removal of the surfactant of the Teflon suspension the temperature was raised to 250 °C with a heating rate of 1 °C/h and held for 2 h. Sealing of the graphite was achieved at 270 °C for 1 h with a heating rate of 1 °C/h. The coated graphite plates were polished (rotating bristles brush, 7000 rpm), washed with deionised water and kept in a vacuum dryer under reduced pressure for 16 h. Before the first measurement, the Teflon coatings on the catalyst support areas were removed using a special drill (8 mm diameter). The removal of the Teflon coating was controlled using a resistance meter.

2.5. Coating of working electrode spots

For the coating of the electrode spots, 5 ± 0.15 mg of the catalysts were dispersed for 10 min in a mixture of ethylene glycol and water (7:3, mass concentration: 0,35 mg/30 μl), using an ultrasonic bath (MK 100, Bandelin). 30 μl of the catalyst dispersion was pipetted directly from the dispersion vial positioned in the ultra sonic bath to the catalyst support area on the working electrode array. The removal of the ethylene glycol water mixture was carried out in a vacuum oven at room temperature for 1 h at 0.2 bar followed by 16 h at 10^{-3} mbar.

After drying of the catalyst coatings, 10 μl of a 0.05% Nafion solution in isopropanol (Standard: Nafion 117 solution, 5%; Sigma–Aldrich) were pipetted on top of each of the catalyst coatings and dried for 20 min in an argon flow. The achieved coatings were rinsed with water for 5 h by filling the wells of the working electrode with 500 μl of deionised water. Before the measurement, the water was removed by the use of a water-driven pump.

2.6. Fluorescence intensity measurement

2.6.1. Pretest of the high-throughput setup by optical images

The pretests were carried out in a darkroom using a polychrome CCD camera (Ixus 40, Canon) positioned perpendicular to the working electrode array, which was connected to the potentiostat via a platinum foil positioned below the electrode array. Images were obtained manually after a holding time of 1 min at potentials between 450 and 850 mV vs. SHE in steps of 10 mV. The UV lamp was positioned as close as possible to the camera objective to guarantee a uniform illumination of the working electrode array. The counter electrode was separated from the reference electrode/working electrode compartment by three electrolyte bridges.

2.6.2. High-throughput fluorescence intensity measurement setup and modifications for single material measurement

High-throughput fluorescence intensity measurements were carried out in a tailor-made wooden box impermeable to light. A digital high-resolution monochrome 12-bit CCD camera (Retiga 4000 R, Q Imaging) equipped with a lens (TAM 25-HB/12, Tamron) and band-eliminition filter (E 420 LP, Chroma Technology Corp.) was positioned perpendicular to the plane of the graphite plate. The UV lamp was placed next to the camera lens to ensure a uniform illumination of the working electrode array. A copper foil positioned below the working electrode array was used for connection to the potentiostat. Reproducible contact and exact positioning of the working electrode array towards the camera were guaranteed by two location screws in combination with a positioning aid. The counter electrode was separated from the reference electrode/working electrode compartment by five electrolyte bridges.

For single material measurements, in addition to the setup described above, hand-cut frits (4 mm × 4 mm × 2 mm, porosity 1, blanks purchased from Robu Glasfiltergeräte GmbH) were positioned in the channels surrounding the vials of interest.

2.6.3. Data acquisition, processing and analysis

2.6.3.1. Pre-screening for acid stability and test of the high-throughput setup. Images were acquired manually. No further data processing of the images was carried out.

2.6.3.2. High-throughput fluorescence intensity measurement setup. Images were automatically acquired and processed using a PC and commercial imaging software (Image-Pro Plus, Media Cybernetics). The potentiostat was controlled by a tailor-made Labview application. Images were obtained after a holding time of 1 min at potentials between 300 and 1000 mV in steps of 10 mV and between the 1000 and 1175 mV vs. SHE in steps of 25 mV. Additionally, an image for background subtraction was acquired at the beginning of the measurement. Using Image-Pro Plus software, 60 areas of interests (AOI) in each image according to well positions were defined. A bitmap analysis for each AOI was carried out. The summation of the obtained greyscale values for each pixel was realized using a commercially available spreadsheet calculation software, resulting in intensity values with arbitrary units for each well and potential, respectively. For data analysis, the intensity values were plotted against the potential vs. SHE. The automation of data analysis was achieved by the use of macro software tool (MacroTools Works, Pitrinec Inc.).

2.7. Cyclic voltammetry (CV)

The cyclic voltammetry experiments were carried out at 25 °C in a three-electrode cell. An oxygen free (purged with argon) 0.5 M H_2SO_4 solution containing 1 M methanol was used as electrolyte for methanol-oxidation experiments. The anodes were prepared as described above on glassy carbon sticks (5 mm in diameter, 50 mm in length). The sticks were mounted in a Teflon holder containing a gold tip as current collector. A Pt-wire was used as counter electrode. The measurements were carried out with a scanrate of 20 mV/s.

3. Results and discussion

The goal of the project was to develop a HT-technology, which allowed to screen for potential anode catalysts of unlimited composition. For catalyst synthesis the versatile sol–gel methods were chosen. For rapid and simple quantification of electrochemical

properties fluorescence was selected. In order to separate the fluorescence of individual materials for quantification, the library had to be composed of separated compartments for each catalyst. Graphite, which lends itself well for machining and CCD-processing and has a high conductivity (graphite electrodes) was chosen as library material and working electrode at the same time. In order to reduce the number of potential catalyst candidates it was essential to exclude all materials not stable under acidic conditions. For rapid identification of such acid sensitive materials, a simple screening method had to be developed.

3.1. Optical pre-screening for acid stability

The stability of a catalyst in the acidic environment of MEA with a pH of ~1 is of paramount importance. In the high–throughput screening process for new DMFC catalysts based on automated sol–gel synthesis, electrochemical measurements are bottle necks. Pre-selection of unsuitable materials before electrochemical evaluation thus accelerates the process. Therefore we developed a fast, parallel optical pre-screening based on the use of translucent 96-well plates, an orbital shaker and a simple document scanner to rapidly identify acid sensitive candidates among the freshly synthesized materials for elimination. The materials were filled into the 96-well plates. Images were acquired after defined time intervals (over a period up to 72 h) of the first contact with a 1 M H_2SO_4 solution (Fig. 2a). For the identification of acid instability, four exclusion criteria were defined: complete solubility, discoloration of the H_2SO_4 solution, hydrogen development and discoloration of the material. Fig. 2b–e illustrates the optical appearance of all four criteria. A set of 1310 materials, binary and ternary mixed oxides of eleven transition metals and in oxidized an reduced form (H_2 at 450 °C) were screened for acid stability. With this pre-screening method 134 materials were identified as acid stable regarding the defined stability criterions, which amounts to an effective sample reduction by 90%. None of the 134 materials showed any significant activity towards methanol oxidation in subsequent electrochemical oxidation experiments. The described pre-screening principle is presently used for materials with a low noble metal content.

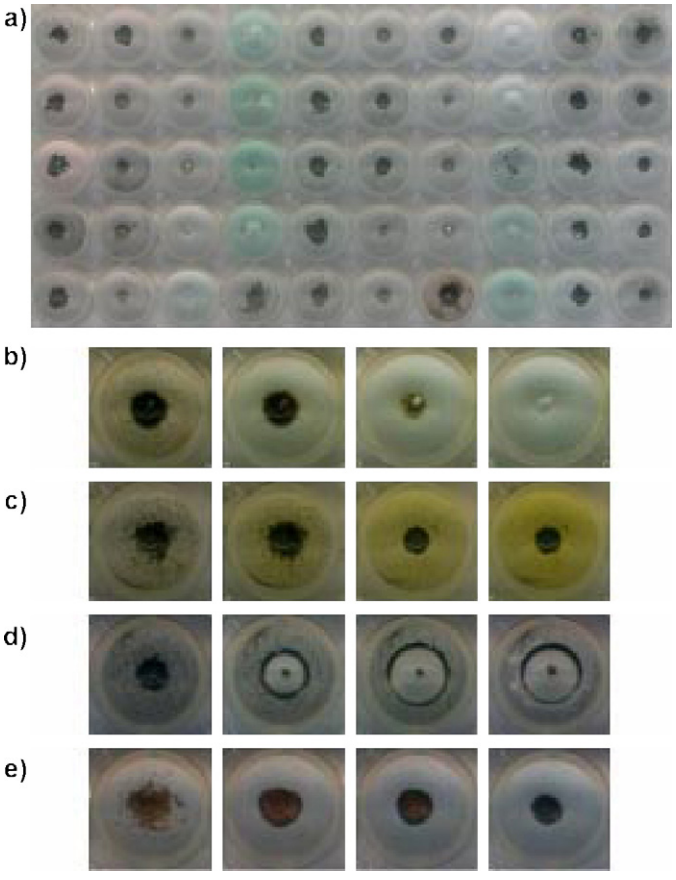

Fig. 2. Pre-screening for acid stability: (a) well-plate filled with 50 materials and 1 M H_2SO_4 after a contact time of 72 h; exclusion criteria (b) complete solubility, (c) discoloration of the H_2SO_4 solution, (d) hydrogen development and (e) discoloration of the material; images acquired directly after the contact between the material and the acid and after 1, 3, and 24 h.

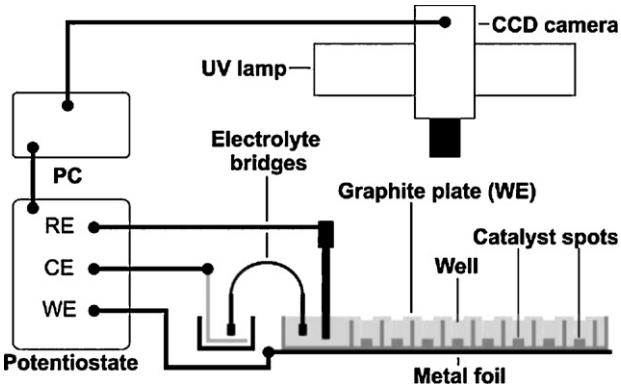

Fig. 3. Schematic drawing of the HT setup; working electrode (WE), counter electrode (CE), reference electrode (RE).

3.2. Primary design of the working electrode and coating with sol–gel derived materials

As already mentioned graphite electrode material was chosen as working electrode; it is affordable, conducting and can be machined to accommodate catalysts and electrolytes. The size and depth of the individual compartments for the catalysts, the positioning of the reference, and counter electrodes had to be clarified first, as well as the number of counter electrodes that are necessary and if several catalysts can be monitored with one set of electrodes and up to what distance they can be arranged. In other words, for the final design of the working electrode library some pretesting was required (Fig. 3). The working electrode was prepared from solid graphite plates, commercially available as graphite electrode materials. The first problem encountered was a graphite material, which showed intensive fluorescence under potential scans with methanol in the absence of any catalyst material. The binder used by the manufacturer for the electrode preparation could be identified as the origin of this unacceptable fluorescence. Binder free graphite electrodes are also commercially available, but they are porous, which lead to leakage during potential scans. After coating of the machined graphite surface with Teflon, the problem was solved and a usable working electrode was obtained. For deposition of the catalyst films, however, the catalyst support areas had to be made Teflon free. This was accomplished by cutting with the CNC-robot about a 10th of a millimeter from the surface of each support area in the wells. The rather viscous catalyst dispersion could now be deposited properly and dried.

So far, conductive materials chosen for the working electrode in screening setups based on the principle reported by Reddington et al. [95] were carbon paper sheets [87,91], indium–tin oxide layers [79] and metallic sputtering targets [28,53,58,66]. Those substrates were coated in situ by impregnation or sputtering to produce the catalyst libraries. In this work, catalysts were obtained as powders by sol–gel processes, followed by reduction in hydrogen. Therefore, synthesis and coating of the working electrode are

separate steps. The separation of catalyst synthesis and coating allows the screening of catalyst in powder form obtainable from a variety of synthesis techniques, such as sol–gel synthesis, impregnation, precipitation, flame spray pyrolysis and others. In order to form uniform coatings of catalysts consisting of highly diverse elemental compositions and therefore characteristics, powders were dispersed in a mixture of ethylene glycol and water using an ultrasonic bath. The main advantage of this mixture is its high surface tension. When pipetted on a surface with well-defined borders (catalyst support area), the dispersion forms stable and easy to handle drops on the surface of the substrate. Therefore the catalyst compartments in the graphite library were drilled into the solid with the bottom as support for the catalyst film. In order to avoid interactions of the film with the compartment walls and to create the defined borders around the mentioned above, the well bottoms were surrounded by grooves, as can be seen in Fig. 4. After deposition of the catalyst dispersions onto the catalyst support areas, due to its high boiling point the dispersion medium ethylene glycol has to be removed under reduced pressure to obtain the catalyst coatings.

Fig. 4a and b show the geometry of the first structured graphite library used for pretesting. It contains a variety of different catalyst spot geometries. The optimal catalyst spots size was found to be 5 mm in diameter in the case of a pipetting volume of 30 μl and a catalyst concentration of 0.35 mg/30 μl of the catalyst. It was found that due to diffusion of the fluorescent dye formed the quantification of fluorescence was most reliable in the deep wells.

A variety of dispersions pipetted onto the 5 mm graphite catalyst support in suspended and in dried form are shown in Fig. 4c and d, respectively, as photographic images. Fig. 5 shows microscope images of randomly selected catalyst films in the wells. In the lower left of each image a part of catalyst film was removed mechanically to also show the surface of the graphite support area. The ablation of the catalyst coating during measurement was prevented by pipetting a 0.05% nafion solution in isopropanol onto the catalyst coatings. After the evaporation of the alcohol and watering of the formed thin Nafion membrane, no catalyst particles got removed during the whole measurement contact time of 80 min between the catalyst/nafion layer and the electrolyte. Although known for its acidic properties, the nafion coating on the graphite spots effected no increase in base fluorescence of the electrolyte as proven by control experiments.

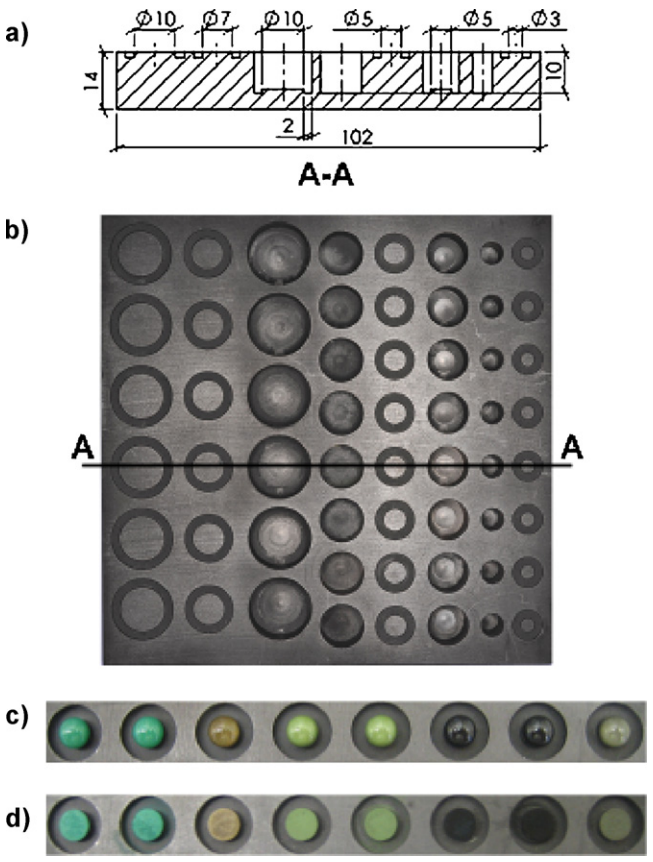

Fig. 4. Variations of catalyst spot geometries, (a) section view (line A–A) of the graphite plate, shown in (b), (c) catalyst dispersions pipetted on 5 mm spots, (d) catalyst coatings after drying under reduced pressure.

3.3. *Pretesting for the development of high-throughput fluorescence screening*

For pretesting all catalyst support areas were coated with identical amounts of the $Pt_{50}Ru_{50}$ catalyst and the library plate was immersed completely in electrolyte. In the first setup it was attempted to position the Pt-counter electrode in the form of a Pt-net over all wells of the working electrode plate. In addition to

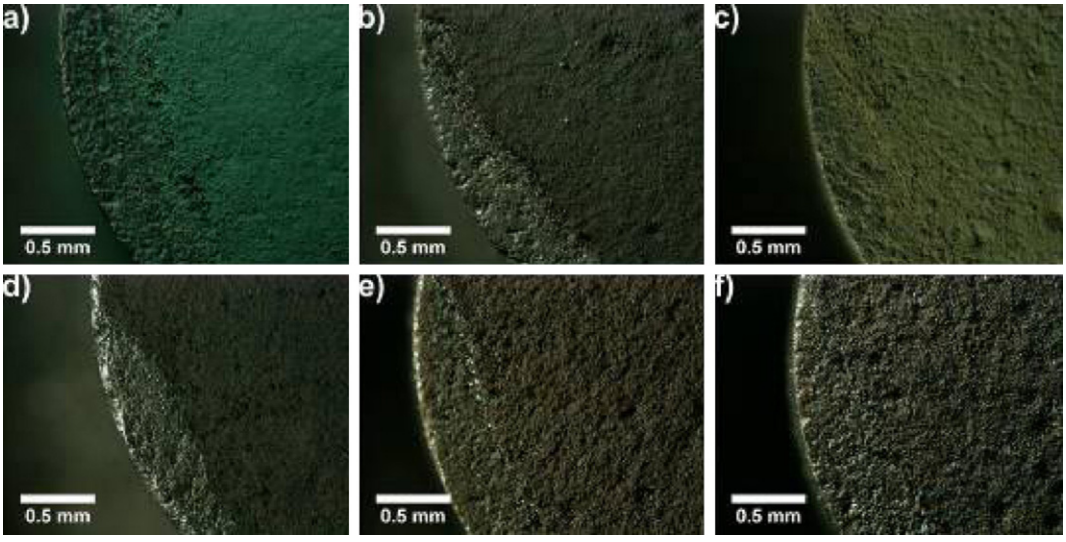

Fig. 5. Reflected light microscope images of coated catalyst on 5 mm spots (magnification: 50); catalyst layer on the lower left on each spot removed to show the surface of the graphite plate: (a) $Co_{25}Cr_{75}$, (b) CoCrCu, (c) $Cu_{25}Cr_{75}$, (d) $Cu_{25}Mo_{75}$, (e) $Fe_{75}Mn_{25}O_x$, (f) $Mn_{50}Zr_{50}O_x$.

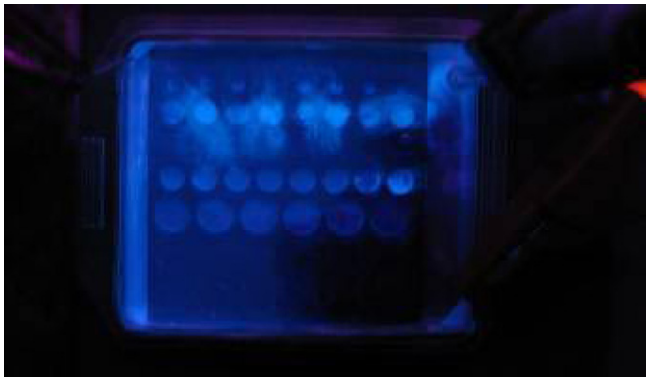

Fig. 6. Advance setup; quenching of the basic fluorescence of the electrolyte in the counter electrode area at 670 mV vs. SHE (bottom right); light circular areas coated with $Pt_{50}Ru_{50}$; (top right) reference electrode; (top left) contacting of the working electrode

observable fluorescence in the wells, the whole area of the counter electrode started to glow at a potential of 200 mV. Apparently the Pt of the counter electrode leads also to fluorescence at lower potentials, which rendered this approach useless. In a 2nd attempt the net was replaced by Pt-foil positioned in the corner of the electrolyte compartment. With this arrangement the basic fluorescence of the electrolyte was quenched at higher potentials as can be seen in the right bottom in Fig. 6 (photographic image, counter electrode in the bottom right, reference electrode positioned upper right, connection to working electrode upper left). This effect was reproduced also with gold, palladium and indium counter electrodes foils. In addition, Fig. 6 shows that the diffusion of the fluorescent dye was hindered and concentrated in the graphite plate wells during the measurement.

To overcome these setbacks, the counter electrode was separated from the working electrode and the reference electrode compartment by electrolyte bridges (Fig. 7). Instead of immersing the working electrode completely into the electrolyte, channels were cut into the graphite plate connecting all catalyst wells with the reference electrode compartment (see Fig. 8). This structured graphite plate includes the compartment for the reference electrode, which is surrounded by various channels of electrolyte channels, which connect various arrays of catalyst wells in different distances. The counter electrode (Pt-wire) is connected to the reference electrode compartment via 3 electrolyte bridges as shown

Fig. 7. From the reference/working electrode (right) compartment separated counter electrode (right); Separation was realized by the use of three electrolyte bridges (middle).

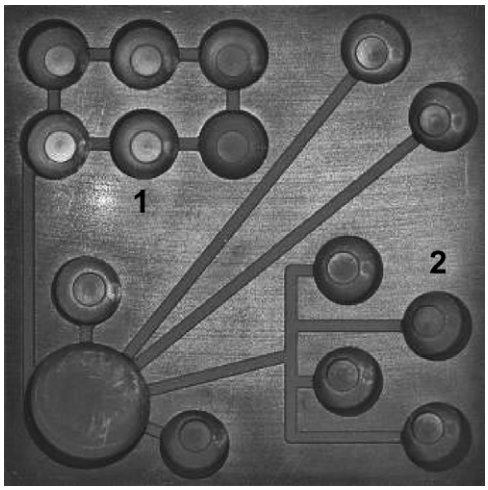

Fig. 8. Graphite plate design for the proof of principle (75 mm × 75 mm), (bottom left) compartment for the reference electrode; (top left, bottom right) basic vial arrangements (1, 2), (bottom left to top right) vial arrangement for the visualisation of the dependence of the fluorescent dye development on the channel length.

in Fig. 7. The progress of fluorescence development during potential increase as recorded with a simple digital camera is shown in Fig. 9. At low potentials identical fluorescence was observed above all catalyst wells. At 650 and 750 mV a small difference of the fluorescence intensity depending on the channel length between the wells and the electrode compartment can be identified. The most identical development of the fluorescence is seen only in the well array 1 (see also Fig. 9). The tendency of dye diffusion to neighbouring wells is documented in Fig. 10. Here only the lower right well of array 1 contains the PtRu catalyst. It took about 40 min, before significant fluorescence became detectable in the neighbouring wells, which allows to place such densely packed arrays on the library.

3.4. Design of the high-throughput library for fluorescence measurements

3.4.1. The components

The design of the final library (=working electrode array) is shown in Fig. 11. It is basically composed of the reference electrode compartment on the lower left surrounded by four well arrays, containing three times 16 and one time 12 wells (diameter 5 mm, depth 9 mm, catalyst support diameter 4 mm). The wells are interconnected through shallow channels (4 mm wide and 2 mm deep). To improve electric contact, 6 additional channels (12 mm deep, 3 mm wide), starting from the reference electrode compartment go around the well arrays and interconnect through the middle of the library (Fig. 11). With this library design a maximum of 60 catalysts can be screened in parallel.

For fluorescence quantification the design of the working electrode is as important as the standardization of the illuminating conditions. For the elimination of external light sources, all the components were enclosed in a light-tight wooden box sealed with a double-layered door (Fig. 12a). The power supply and data connection of the camera and the contact of the three electrodes with the potentiostat were fed through light locks situated underneath the working electrode. The optical opaqueness of the wooden box was controlled by a light meter (0 W m^{-2}). The excitation of the protonated quinine was achieved by a UV lamp (15 W) with an emission maximum of 365 nm (emission spectra: 310–400 nm) positioned as close as possible to the perpendicular, centered arranged monochromic 12-bit camera (Fig. 12b and c) above the working electrode array and above the end of the camera lens.

Fig. 9. Proof of principle; formation of the fluorescent dye during methanol oxidation at (a) 550 mV, (b) 650 mV and (c) 750 mV vs. SHE

Excited with light in the range of 340–390 nm, the emission maximum of the protonated quinine (in 0.1 N H_2SO_4) is located between 458 and 466 nm [108,109]. Reflections of the exciting light, originating from setup components and the electrolyte surface (Fig. 10), were eliminated by the use of a band-gap filter with opaqueness up to 420 nm and a transmission degree of 85% for light with the wavelength of 460 nm. To decrease resistance the separation of the counter electrode from the reference electrode compartment was achieved by five electrolyte bridges (Fig. 12d and e).

3.4.2. Determination of the exposure time, data analysis and correction of the optical system

Because of the application of a 12-bit monochromic camera, 4096 grey scales per pixel could have been used as intensity range of the fluorescence. To avoid overexposure of the images acquired during the measurements, a graphite plate was filled with the electrolyte, acidified by four equivalents of sulfuric acid relative to the quinine content to achieve a pH of 1. At this pH, the quinine is completely transferred to its doubly protonated dication [109–111] and no further intensity increase is possible. The optimization of the exposure time was accomplished by mapping the saturation of the grey scales of each pixel in an image while varying the exposure time (Fig. 13). At low exposure times (Fig. 13a), the pixels in the outer ranges of the picture were under exposed (yellow (print version: light gray) false color markings) while at high exposure times (Fig. 13e) underexposed ranges disappeared and overexposed pixel ranges are located in the middle of the pictures (red (print version: dark gray) color markings). The optimal exposure time was found to be 155 ms (Fig. 13c). In the corresponding image, underexposure was limited to outer ranges of the image and a few pixels with overexposure were settled in the middle of the image. With the definition of the exposure time, the system was calibrated to the highest level of fluorescence intensity and the reduced transmission of the band gap filter was counterbalanced.

For the purpose of data analysis, a circular area of interest (AOI) with a constant size was defined over each well position. In each of these AOIs, a bitmap analysis was carried out to obtain the greyscale values of each pixel included. The summation of the greyscale values led to cumulated intensity values in arbitrary units for each of the 60 well positions in all of the images acquired during a measurement. Plotted vs. the applied potentials, the intensity values are interpreted as indicators of methanol conversion during the increase of the potential displayed as signal visible under UV light.

As seen in Fig. 14, the intensity in an image of a graphite plate, equally filled with an acidified electrolyte, exhibits a circular decline from the center to the image margins caused by the used lens. Additionally, evoked by the non-centrically positioned ultra violet lamp, a minor difference in the illumination conditions of each vial can be assumed. To overcome these intensity inconsistencies, a mathematical correction of the optical system

Fig. 10. Dye collection/concentration capability of the vial channel relief. After 40 min the dye starts diffusion in the neighbouring vials. Reflections of the ultra violet lamp on the liquid surface in each vial were removed in the high-throughput setup by the use of a band elimination filter

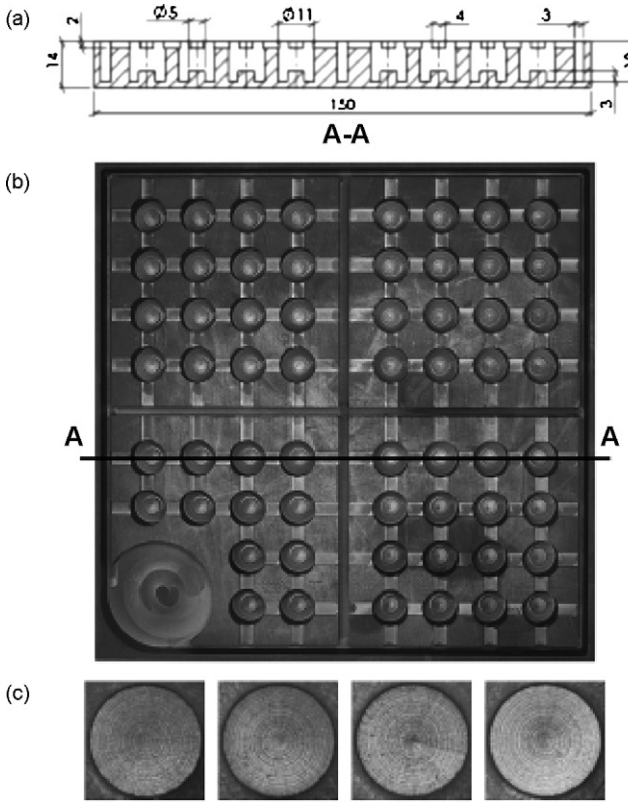

Fig. 11. High-throughput graphite plate design, (a) section view (line A–A) of the graphite plate relief design shown in (b), (c) standardization of the catalyst spot surface topography by the used cleaning process.

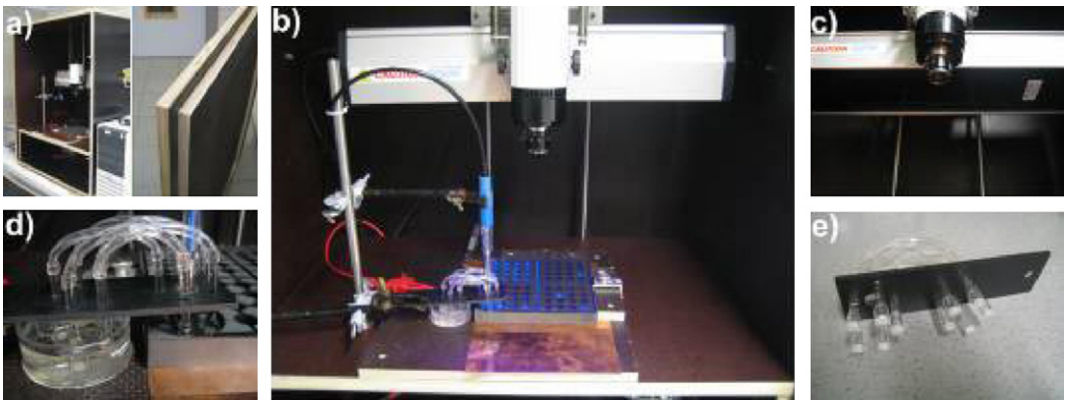

Fig. 12. High-throughput setup: (a) light-tight wooden box (left) with double-layered cover (right), (b) arrangement of screening components: ultraviolet lamp, camera, copper foil for contacting the working electrode, reference/working electrode compartment separated from counter electrode compartment by electrolyte bridges, (c) ultraviolet lamp/camera arrangement, (d) separation of the counter electrode (left) from the reference/working electrode compartment. (e) Holder for five electrolyte bridges.

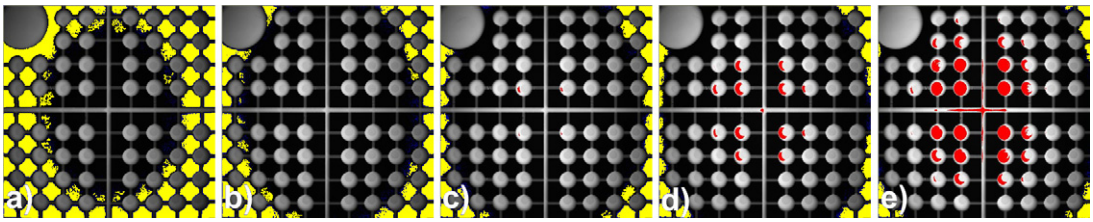

Fig. 13. Determination of the optimal exposure time by mapping the saturation of the greyscales of each pixel while varying the exposure time, (a) 100 ms, (b) 130 ms, (c) 155 ms, (d) 170 ms, (e) 200 ms, yellow (print version: light gray): 0 (black), red (print version: dark gray): 4095 (white).

components was implemented. For the calculation of correction factors for each vial position, images of graphite plates, filled with electrolytes, acidified with varying amounts of H_2SO_4, were acquired. The correction factors were obtained by relation of the calculated intensities to the well position with the maximum intensity value marked by the light cycle in Fig. 14a–d in each image. Fig. 15 shows a mapping of the average correction factors and the standard deviations depending on the well position on the graphite plate. For validation of the correction factors, a graphite plate filled with an electrolyte was acidified with a random amount of H_2SO_4. For the corrected intensities of the 60 vial positions, a standard deviation of 4% was obtained.

3.4.3. *Automation of data acquisition and data analysis*

The automation of both, data acquisition and data analysis was achieved by the combination of different kinds of software. Fig. 16 shows the software relationships. For the data acquisition, a home made control software was used, which allowed the stepwise increase of the potential vs. SHE. Time programmed acquisition of the images after each potential step was achieved by the use of the image processing software (Image-Pro Plus). A macro tool executed the simultaneous start of the potential program flow and the image acquisition sequence. The image processing tool allowed the automation of background subtraction and bitmap analysis of the 60 well positions for each image acquired. Without the coordinating macro tool, the bitmap analysis would have to be carried out manually image-by-image, because of the lack of two-way communication between the image processing software and the spreadsheet calculation program used for intensity calculations. In addition, the macro tool was used for automated data accumulation and data storage.

3.5. *Validation of the high-throughput screening system*

For validation of the high-throughput setup, the catalyst supports in the 60 wells on the graphite plate were coated with the same amount of the $Pt_{50}Ru_{50}$ catalyst. During the increase of the potentials, the first development of fluorescence was optically determined at 470 mV. The fluorescence observed in all of the 60 vials was identical. For the creation of a comparability criterion, two regression analyses were carried out: one in the range between 300 and 400 mV and the other in the range between 650 and 750 mV

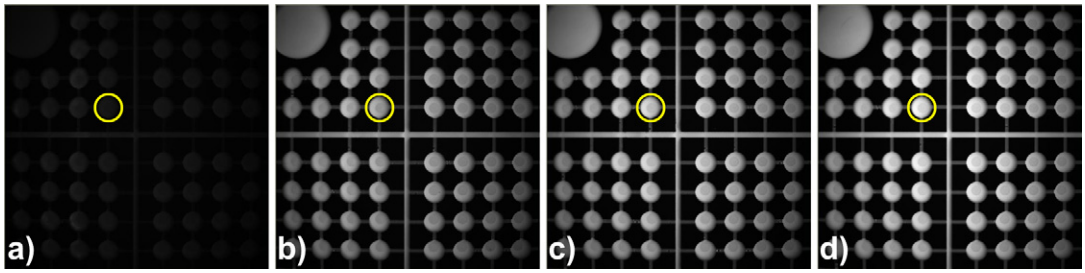

Fig. 14. Images of the graphite plate filled with electrolyte acidified with different amounts of H_2SO_4: (a) non-acidified, (b) one equivalent, (c) two equivalents, (d) four equivalents referred to the quinine content.

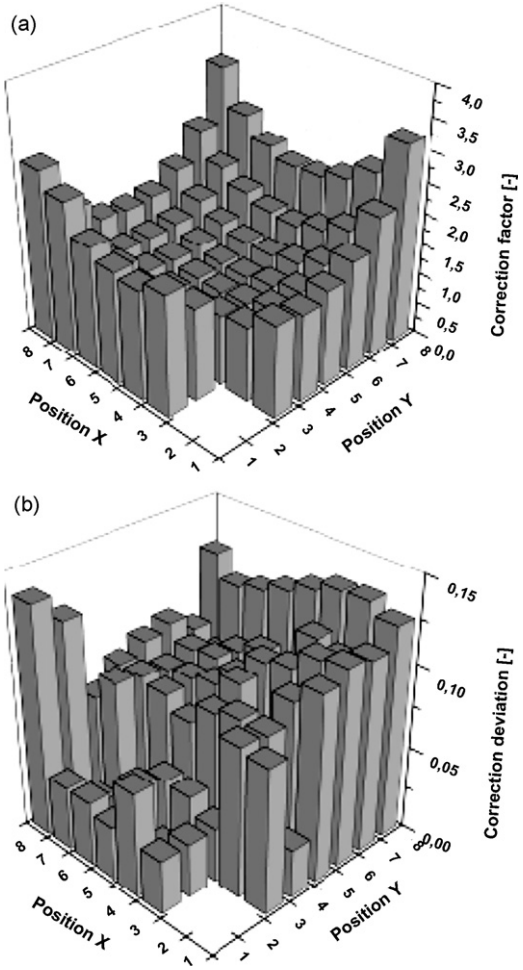

Fig. 15. Mapping of the correction factors (a) and standard deviations ($n = 4$) depending on the vial position on the graphite plate.

(Fig. 17). The abscissa of the intersection point of the two regression lines was defined as the so-called calculated onset of the fluorescence development. The mean value for the calculated onset was obtained with a standard deviation of 2%, which shows a high reproducibility of the fluorescence onset of the 60 catalyst spots.

The system still suffered under the deviations of fluorescence intensity of identical catalyst spots ($Pt_{50}Ru_{50}$) at higher potentials as illustrated with the intensity plots of 2 reference catalysts in Fig. 18 (empty squares and circles). Diffusion effects of dye from well to well could be identified as origin of the deviation at higher

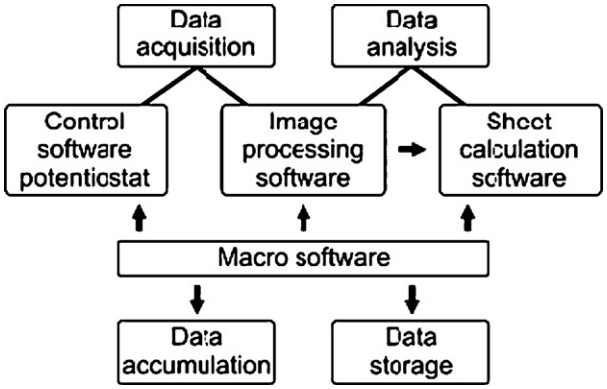

Fig. 16. Overview over software and software relationships (lines) used for data acquisition and analysis—arrows show possible data transfer.

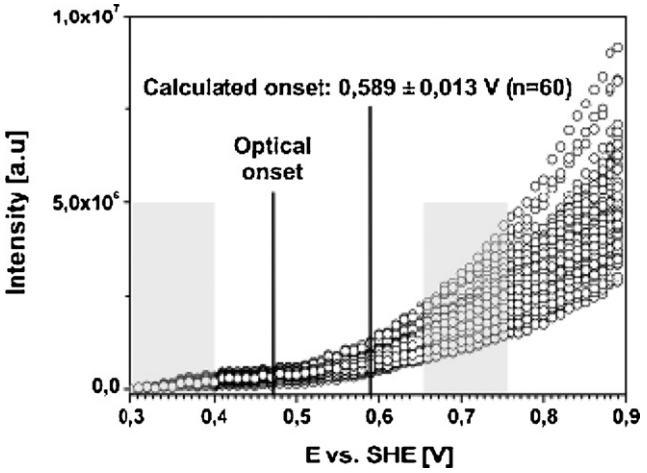

Fig. 17. Enlarged onset regions, ranges of the two linear regression regions marked in grey.

potentials. The problem could be eliminated by positioning of small frits in the channels between the wells as illustrated in Fig. 19. Not only were the plots obtained from the 2 wells now identical (see Fig. 18, filled squares and circles), but also the intensity increased rendering the setup more sensitive. The regression ranges were the same used for the high-throughput measurement. The mean value of the calculated onsets in the frit-supported measurement varied 21 mV (4%) from the value obtained at the high-throughput measurement. The standard deviation of the calculated onsets is about 1%, which documents the reproducibility of all the pre-measurement procedures, such as the coating procedure. Due to the large resistance introduced in the case of filling all the channels with frits, this method was only used for single material measurements, not for array measurements.

Fig. 20 shows a comparison of the methanol-oxidation current density and fluorescence intensity of $Pt_{50}Ru_{50}$. Measured in 0.5 M H_2SO_4, the onset of the current density (measured in a conventional cyclic voltammetry setup) shows a shift of about 60 mV to lower potentials compared with the optical fluorescence intensity onset. Starting from a pH of ~6, the pH of the electrolyte solution used in the fluorescence measurements has to be reduced to a lower value by the protons produced during methanol oxidation resulting in an increase of the concentration of the protonated dication, which is responsible for the fluorescence under UV light [110,111]. In contrast to the CV measurements, the fluorescence intensity

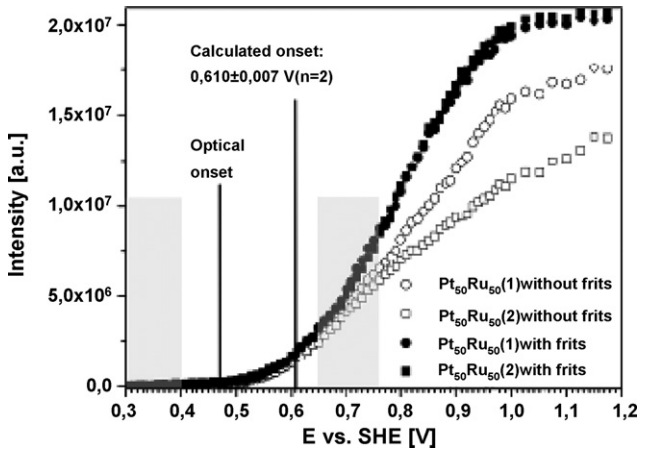

Fig. 18. Effect of the used frits on the fluorescence measurement. Ranges of the two linear regression regions marked in grey.

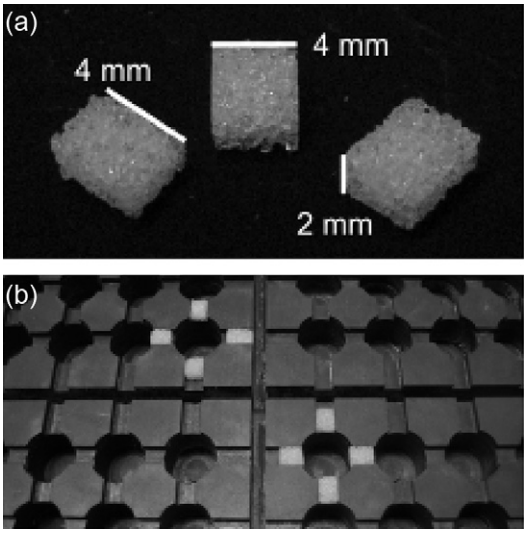

Fig. 19. Frits used for conventional measurements (a); frits positioned in the surrounding channels of the graphite plate relief (b).

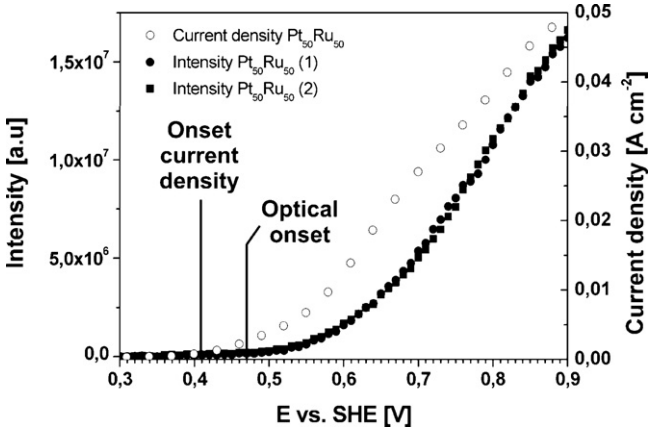

Fig. 20. Comparison of the magnified onset region of intensity and current density (geometric anode area: 0.20 cm^2) of $Pt_{50}Ru_{50}$ measured during the methanol oxidation. The current density was measured in 0.5 M H_2SO_4 solution.

measurement is therefore also dependent on the kinetics of the protonation reaction of the quinine. This leads to an increase of the optical fluorescence onset. Nevertheless, the two onsets are in the same magnitude. The onset of the fluorescence intensity allows an estimation of the current onsets in conventional CV experiments. It has been shown, that potential dependent fluorescence measurements, if carried out carefully, correlate well with conventional CV measurements. Thus, fluorescence measurements, which are much simpler to carry out with arrays in parallel, provide a suitable means to evaluate potential electrodes in high-throughput modes.

4. Conclusion

The objective of the work described here was the development of two high-throughput setups in the field of direct methanol fuel cell catalysts and beyond. For the pre-screening of a broad variety of catalyst powders as potential anode catalysts for acid stability a simple optical method has been developed. Based on four elimination criterions, about 1170 materials out of a test set of 1300 materials were identified as acid instable, reducing the number of materials to be tested electrochemically by 90%. After proper pretesting and suitable control experiments a library design for parallel testing of up to 60 potential electrode catalysts for methanol oxidation by screening of the fluorescence of quinine was developed. The electrode compartment of the presented design is positioned in the lower left corner of the graphite plate. It can easily be anticipated that the graphite plate can be increased to house up to 240 wells, if the electrode compartment is positioned in the middle of a centrosymmetric design. The optical detection of the performance of electrode arrays is low cost and much simpler than the alternative electrochemical setup based on parallel CV measurements with arrays of counter electrodes. Another charm of the method is its versatility with respect to potential catalysts, since all catalysts accessible as powders can be tested. The system was validated by coating a $Pt_{50}Ru_{50}$ catalyst onto the 60 spots of the working electrode array. The standard deviation of the mean value of the calculated fluorescence onsets was 4% ($n = 60$).

Acknowledgments

The authors would like to thank R. Richter and J. Kriesamer for the planning and machining of the main components of the setup and for getting the images of the diverse graphite plate designs. We also thank the metal shop of the physical chemistry.

References

[1] K.A. Mauritz, R.B. Moore, Chem. Rev. 104 (2004) 4535–4585.
[2] M. Lefevre, J.P. Dodelet, P. Bertrand, J. Phys. Chem. B 106 (2002) 8705–8713.
[3] A. Hamnett, Catal. Today 38 (1997) 445–457.
[4] M.P. Hogarth, G.A. Hards, Platinum Met. Rev. 40 (1996) 150–159.
[5] H.S. Liu, C.J. Song, L. Zhang, J.J. Zhang, H.J. Wang, D.P. Wilkinson, J. Power Sources 155 (2006) 95–110.
[6] E.S. Smotkin, R.R. Diaz-Morales, Annu. Rev. Mater. Res. 33 (2003) 557–579.
[7] M.P. Hogarth, T.R. Ralph, Platinum Met. Rev. 46 (2002) 146–164.
[8] M. Watanabe, S. Motoo, J. Electroanal. Chem. Interfacial Electrochem. 60 (1975) 267–273.
[9] H.A. Gasteiger, N. Markovic, P.N. Ross, E.J. Cairns, J. Electrochem. Soc. 141 (1994) 1795–1803.
[10] J.Y. Kim, Z.G. Yang, C.C. Chang, T.I. Valdez, S.R. Narayanan, P.N. Kumta, J. Electrochem. Soc. 150 (2003) A1421–A1431.
[11] W.D. King, J.D. Corn, O.J. Murphy, D.L. Boxall, E.A. Kenik, K.C. Kwiatkowski, S.R. Stock, C.M. Lukehart, J. Phys. Chem. B 107 (2003) 5467–5474.
[12] Y.H. Lee, G. Lee, J.H. Shim, S. Hwang, J. Kwak, K. Lee, H. Song, J.T. Park, Chem. Mater. 18 (2006) 4209–4211.
[13] J.T. Moore, J.D. Corn, D. Chu, R.Z. Jiang, D.L. Boxall, E.A. Kenik, C.M. Lukehart, Chem. Mater. 15 (2003) 3320–3325.
[14] J.C. Huang, Z.L. Liu, C.B. He, L.M. Gan, J. Phys. Chem. B 109 (2005) 16644–16649.
[15] B.H. Wu, D. Hu, Y.J. Kuang, B. Liu, X.H. Zhang, J.H. Chen, Angew. Chem. Int. Ed. 48 (2009) 4751–4754.
[16] Z. Tang, G. Lu, J. Power Sources 162 (2006) 1067–1072.
[17] J.S. Choi, W.S. Chung, H.Y. Ha, T.H. Lim, I.H. Oh, S.A. Hong, H.I. Lee, J. Power Sources 156 (2006) 466–471.
[18] C.T. Hsieh, J.Y. Lin, J. Power Sources 188 (2009) 347–352.
[19] S.L. Gojkovic, J. Serb. Chem. Soc. 68 (11) (2003) 859–870.
[20] L. Colmenares, E. Guerrini, Z. Jusys, K.S. Nagabhushana, E. Dinjus, S. Behrens, W. Habicht, H. Bonnemann, R.J. Behm, J. Appl. Electrochem. 37 (2007) 1413–1427.
[21] G. Chen, D.G. Xia, Z.R. Nie, Z.Y. Wang, L. Wang, L. Zhang, J.J. Zhang, Chem. Mater. 19 (2007) 1840–1844.
[22] E. Antolini, J.R.C. Salgado, E.R. Gonzalez, Appl. Catal. B 63 (2006) 137–149.
[23] S.A. Lee, K.W. Park, J.H. Choi, B.K. Kwon, Y.E. Sung, J. Electrochem. Soc. 149 (2002) A1299–A1304.
[24] Z.B. Wang, G.P. Yin, J. Zhang, Y.C. Sun, P.F. Shi, Electrochim. Acta 51 (2006) 5691–5697.
[25] T.C. Deivaraj, J.Y. Lee, J. Electrochem. Soc. 151 (2004) A1832–A1835.
[26] F. Liu, J.Y. Lee, W.J. Zhou, Small 2 (2006) 121–128.
[27] P.K. Shen, C.W. Xu, R. Zeng, Y.L. Liu, Electrochem, Solid State Lett. 9 (2006) A39–A42.
[28] J.M. Gregoire, M. Kostylev, M.E. Tague, P.F. Mutolo, R.B. van Dover, F.J. DiSalvo, H.D. Abruna, J. Electrochem. Soc. 156 (2009) B160–B166.
[29] A.O. Neto, J. Perez, W.T. Napporn, E.A. Ticianelli, E.R. Gonzalez, J. Braz. Chem. Soc. 11 (2000) 39–43.
[30] M. Barroso de Oliveira, L.P.R. Profeti, P. Olivi, Electrochem. Commun. 7 (2005) 703–709.
[31] C. Song, M. Khanfar, P.G. Pickup, J. Appl. Electrochem. 36 (3) (2006) 339–345.
[32] Y.J. Gu, W.T. Wong, J. Electrochem. Soc. 153 (2006) A1714–A1718.
[33] H.M. Villullas, F.I. Mattos-Costa, L.O.S. Bulhoes, J. Phys. Chem. B 108 (2004) 12898–12903.
[34] J.H. Choi, K.W. Park, I.S. Park, W.H. Nam, Y.E. Sung, Electrochim. Acta 50 (2004) 787–790.
[35] G. Chang, M. Oyama, K. Hirao, J. Phys. Chem. B 110 (2006) 1860–1865.

[36] K.J. Cathro, J. Electrochem. Soc. 116 (1969) 1608.
[37] K. Ke, K. Waki, J. Electrochem. Soc. 154 (2007) A207–A212.
[38] Z.D. Wei, L.L. Li, Y.H. Luo, C. Yan, C.X. Sun, G.Z. Yin, P.K. Shen, J. Phys. Chem. B 110 (51) (2006) 26055–26061.
[39] I. Honma, T. Toda, J. Electrochem. Soc. 150 (2003) A1689–A1692.
[40] M.A.A. Rahim, M.W. Khalil, H.B. Hassan, J. Appl. Electrochem. 30 (2000) 1151–1155.
[41] T. Frelink, W. Visscher, J.A.R. Vanveen, Surf. Sci. 335 (1995) 353–360.
[42] K. Wang, H.A. Gasteiger, N.M. Markovic, P.N. Ross, Electrochim. Acta 41 (1996) 2587–2593.
[43] L.J. Zhang, D.G. Xia, Appl. Surf. Sci. 252 (2006) 2191–2195.
[44] G. Gokagac, B.J. Kennedy, Z. Naturforsch. B: J. Chem. Sci. 57 (2002) 193–201.
[45] C.M. Johnston, S. Strbac, A. Lewera, E. Sibert, A. Wieckowski, Langmuir 22 (2006) 8229–8240.
[46] H. Tsaprailis, V.I. Birss, Electrochem. Solid-State Lett. 7 (2004) A348–A352.
[47] J.H. Choi, K.W. Park, I.S. Park, K. Kim, J.S. Lee, Y.E. Sung, J. Electrochem. Soc. 153 (2006) A1812–A1817.
[48] J.H. Choi, K.J. Jeong, Y. Dong, J. Han, T.H. Lim, J.S. Lee, Y.E. Sung, J. Power Sources 163 (2006) 71–75.
[49] M. Watanabe, S. Motoo, J. Electroanal. Chem. Interfacial Electrochem. 60 (1975) 259–266.
[50] Y.B. Lou, M.M. Maye, L. Han, J. Luo, C.J. Zhong, Chem. Commun. (2001) 473–474.
[51] X.B. Ge, R.Y. Wang, P.P. Liu, Y. Ding, Chem. Mater. 19 (2007) 5827–5829.
[52] S. Kumar, S.Z. Zou, Langmuir 23 (2007) 7365–7371.
[53] M. Prochaska, J. Jin, D. Rochefort, L. Zhuang, F.J. DiSalvo, H.D. Abruna, R.B. van Dover, Rev. Sci. Instrum. 77 (2006).
[54] S. Papadimitriou, A. Tegou, E. Pavlidou, G. Kokkinidis, S. Sotiropoulos, Electrochim. Acta 52 (2007) 6254–6260.
[55] Z.L. Liu, B. Guo, S.W. Tay, L. Hong, X.H. Zhang, J. Power Sources 184 (2008) 16–22.
[56] C. Roychowdhury, F. Matsumoto, V.B. Zeldovich, S.C. Warren, P.F. Mutolo, M. Ballesteros, U. Wiesner, H.D. Abruna, F.J. DiSalvo, Chem. Mater. 18 (2006) 3365–3372.
[57] J.S. Wang, J.Y. Xi, Y.X. Bai, Y. Shen, J. Sun, L.Q. Chen, W.T. Zhu, X.P. Qiu, J. Power Sources 164 (2007) 555–560.
[58] J.M. Gregoire, R.B. van Dover, J. Jin, F.J. DiSalvo, H.D. Abruna, Rev. Sci. Instrum. 78 (2007).
[59] J.S. Cooper, M.K. Jeon, P.J. McGinn, Electrochem. Commun. 10 (2008) 1545–1547.
[60] M.K. Jeon, J.S. Cooper, P.J. McGinn, J. Power Sources 192 (2009) 391–395.
[61] Z.t. Zhou, W.j. Liu, Dianyuan Jishu 30 (2006) 203–205.
[62] M. Chen, Z.B. Wang, Y. Ding, G.P. Yin, Electrochem. Commun. 10 (2008) 443–446.
[63] K.W. Park, J.H. Choi, Y.E. Sung, J. Phys. Chem. B 107 (2003) 5851–5856.
[64] K. Miyazaki, K. Matsuoka, Y. Iriyama, T. Abe, Z. Ogumi, J. Electrochem. Soc. 152 (2005) A1870–A1873.
[65] X.H. Jian, D.S. Tsai, W.H. Chung, Y.S. Huang, F.J. Liu, J. Mater. Chem. 19 (2009) 1601–1607.
[66] J. Jin, M. Prochaska, D. Rochefort, D.K. Kim, L. Zhuang, F.J. DiSalvo, R.B. van Dover, H.D. Abruna, Appl. Surf. Sci. 254 (2007) 653–661.
[67] J.A. Tian, G.Q. Sun, L.H. Jiang, S.Y. Yan, Q. Mao, Q. Xin, Electrochem. Commun. 9 (2007) 563–568.
[68] A. Lima, C. Coutanceau, J.M. Leger, C. Lamy, J. Appl. Electrochem. 31 (2001) 379–386.
[69] P. Strasser, J. Comb. Chem. 10 (2008) 216–224.
[70] P. Strasser, Q. Fan, M. Devenney, W.H. Weinberg, P. Liu, J.K. Norskov, J. Phys. Chem. B 107 (2003) 11013–11021.
[71] J.S. Cooper, P.J. McGinn, J. Power Sources 163 (2006) 330–338.
[72] J.H. Choi, K.W. Park, B.K. Kwon, Y.E. Sung, J. Electrochem. Soc. 150 (2003) A973–A978.
[73] Z.B. Wang, G.P. Yin, P.F. Shi, Y.C. Sun, Electrochem. Solid-State Lett. 9 (2006) A13–A15.
[74] F. Liu, J.Y. Lee, W.J. Zhou, J. Electrochem. Soc. 153 (2006) A2133–A2138.
[75] T. Huang, D. Zhang, L. Xue, W.B. Cai, A. Yu, J. Power Sources 192 (2009) 285–290.
[76] N. Tsiouvaras, M.V. Martinez-Huerta, R. Moliner, M.J. Lazaro, J.L. Rodriguez, E. Pastor, M.A. Pena, J.L.G. Fierro, J. Power Sources 186 (2009) 299–304.
[77] X. Zhang, F. Zhang, K.Y. Chan, J. Mater. Sci. 39 (2004) 5845–5848.
[78] T. Kawaguchi, Y. Rachi, W. Sugimoto, Y. Murakami, Y. Takasu, J. Appl. Electrochem. 36 (2006) 1117–1125.
[79] S. Jayaraman, A.C. Hillier, Meas. Sci. Technol. 16 (2005) 5–13.
[80] O. Yepez, P.G. Pickup, Electrochemical, Solid State Lett. 8 (2005) E35–E39.
[81] P.J. Barczuk, H. Tsuchiya, J.M. Macak, P. Schmuki, D. Szymanska, O. Makowski, K. Miecznikowski, P.J. Kulesza, Electrochem, Solid State Lett. 9 (2006) E13–E16.
[82] K.L. Ley, R.X. Liu, C. Pu, Q.B. Fan, N. Leyarovska, C. Segre, E.S. Smotkin, J. Electrochem. Soc. 144 (1997) 1543–1548.
[83] S.J. Liao, K.A. Holmes, H. Tsaprailis, V.I. Birss, J. Am. Chem. Soc. 128 (2006) 3504–3505.
[84] P. Sivakumar, V. Tricoli, Electrochem, Solid State Lett. 9 (2006) A167–A170.
[85] Z.X. Liang, T.S. Zhao, J.B. Xu, J. Power Sources 185 (2008) 166–170.
[86] S.Y. Huang, C.M. Chang, C.T. Yeh, J. Catal. 241 (2006) 400–406.
[87] Y.H. Chu, S.W. Ahn, D.Y. Kim, H.J. Kim, Y.G. Shul, H.S. Han, Catal. Today 111 (2006) 176–181.
[88] H.J. Kim, D.Y. Kim, H. Han, Y.G. Shul, J. Power Sources 159 (2006) 484–490.
[89] K.W. Park, J.H. Choi, S.A. Lee, C. Pak, H. Chang, Y.E. Sung, J. Catal. 224 (2004) 236–242.
[90] J.F. Whitacre, T. Valdez, S.R. Narayanan, J. Electrochem. Soc. 152 (2005) A1780–A1789.
[91] W.C. Choi, J.D. Kim, S.I. Woo, Catal. Today 74 (2002) 235–240.
[92] A.S. Arico, Z. Poltarzewski, H. Kim, A. Morana, N. Giordano, V. Antonucci, J. Power Sources 55 (1995) 159–166.
[93] A.S. Arico, P. Creti, N. Giordano, V. Antonucci, P.L. Antonucci, A. Chuvilin, J. Appl. Electrochem. 26 (1996) 959–967.
[94] V. Neburchilov, H.J. Wang, J.J. Zhang, Electrochem. Commun. 9 (2007) 1788–1792.
[95] E. Reddington, A. Sapienza, B. Gurau, R. Viswanathan, S. Saragapani, E.S. Smotkin, T.E. Mallouk, Science 280 (1998) 1735–1737.
[96] B. Gurau, R. Viswanathan, R.X. Liu, T.J. Lafrenz, K.L. Ley, E.S. Smotkin, E. Reddington, A. Sapienza, B.C. Chan, T.E. Mallouk, S. Sarangapani, J. Phys. Chem. B 102 (1998) 9997–10003.
[97] R.R. Diaz-Morales, R.X. Liu, E. Fachini, G.Y. Chen, C.U. Segre, A. Martinez, C. Cabrera, E.S. Smotkin, J. Electrochem. Soc. 151 (2004) A1314–A1318.
[98] E.S. Smotkin, J.H. Jiang, A. Nayar, R.X. Liu, Appl. Surf. Sci. 252 (2006) 2573–2579.
[99] R.Z. Jiang, C. Rong, D. Chu, J. Comb. Chem. 7 (2005) 272–278.
[100] R.X. Liu, E.S. Smotkin, J. Electroanal. Chem. 535 (2002) 49–55.
[101] K.M. Brace, B.E. Hayden, A.E. Russell, J.R. Owen, Adv. Mater. 18 (2006) 3253–3257.
[102] B.C. Chan, R.X. Liu, K. Jambunathan, H. Zhang, G.Y. Chen, T.E. Mallouk, E.S. Smotkin, J. Electrochem. Soc. 152 (2005) A594–A600.
[103] G. Frenzer, W.F. Maier, Annu. Rev. Mater. Res. 36 (2006) 281–331.
[104] H. Shimooka, M. Kuwabara, J. Am. Ceram. Soc. 78 (1995) 2849–2852.
[105] H. Shimooka, M. Kuwabara, J. Am. Ceram. Soc. 79 (1996) 2983–2985.
[106] H. Shimooka, S. Kohiki, T. Kobayashi, M. Kuwabara, J. Mater. Chem. 10 (2000) 1511–1512.
[107] J. Scheidtmann, J.W. Saalfrank, W.F. Maier, Stud. Surf. Sci. Catal. 145 (2003) 13–21.
[108] J.E. O'Reilly, J. Chem. Educ. 52 (1975) 610–612.
[109] R.F. Chen, Anal. Biochem. 19 (1967) 374–386.
[110] S.G. Schulman, R.M. Threatte, W.L. Paul, J. Pharm. Sci. 63 (1974) 876–880.
[111] G. Sontag, G. Kainz, Mikrochim. Acta 2 (1977) 425–436.